Possible quantum fluctuations in the vicinity of the quantum critical point of $(\text{Sr, Ca})_3\text{Ir}_4\text{Sn}_{13}$ revealed by high-energy x-ray diffraction

L. S. I. Veiga ⬤,[1,2] J. R. L. Mardegan,[1] M. v. Zimmermann,[1] D. T. Maimone,[3] F. B. Carneiro,[4,5] M. B. Fontes,[5]
J. Strempfer,[1] E. Granado,[3] P. G. Pagliuso,[3] and E. M. Bittar[5]

[1]*Deutsches Elektronen-Synchrotron (DESY), Hamburg 22607, Germany*
[2]*London Centre for Nanotechnology and Department of Physics and Astronomy, University College London,*
Gower Street, London WC1E 6BT, United Kingdom
[3]*Instituto de Física "Gleb Wataghin", Universidade Estadual de Campinas-UNICAMP, 13083-859 Campinas, São Paulo, Brazil*
[4]*Instituto de Física, Universidade do Estado do Rio de Janeiro, 20550-900 Rio de Janeiro, Rio de Janeiro, Brazil*
[5]*Centro Brasileiro de Pesquisas Física, 22290-180 Rio de Janeiro, Rio de Janeiro, Brazil*

We explore the evolution of the structural phase transition of $(\text{Sr, Ca})_3\text{Ir}_4\text{Sn}_{13}$, a model system to study the interplay between structural quantum criticality and superconductivity, by means of high-energy x-ray diffraction measurements at high pressures and low temperatures. Our results confirm a rapid suppression of the superlattice transition temperature T^* against pressure, which extrapolates to zero at a critical pressure of $\approx 1.79(4)$ GPa. The temperature evolution of the superlattice Bragg peak in $\text{Ca}_3\text{Ir}_4\text{Sn}_{13}$ reveals a drastic decrease of the intensity and an increase of the linewidth when $T \rightarrow 0$ K and $p \rightarrow p_c$. Such anomaly is likely associated with the emergence of quantum fluctuations that disrupt the formation of long-range superlattice modulation. The revisited temperature-pressure phase diagram of $(\text{Sr, Ca})_3\text{Ir}_4\text{Sn}_{13}$ thus highlights the intertwined nature of the distinct order parameters present in this system and demonstrates some similarities between this family and the unconventional superconductors.

DOI: [10.1103/PhysRevB.101.104511](https://doi.org/10.1103/PhysRevB.101.104511)

I. INTRODUCTION

Compounds displaying the interplay between superconductivity (SC) and electronic instabilities have been extensively studied during the past years due to their rich phase diagrams as a function of doping, pressure, or magnetic fields [1–6]. In most cases, SC is found in the vicinity of electronic instabilities of magnetic origin, where the pairing mechanism is mediated by spin fluctuations and the SC is unconventional [7–9]. The proximity of SC to nonmagnetic structural instabilities, on the other hand, is rare, and searches for a quantum critical point (QCP) resulting from a tunable structural phase transition have provoked great interest due to its promising role of stabilizing or even enhancing the pairing mechanism. Thus, accessing SC materials where a detailed study of structural quantum criticality and its impact on SC can be explored is highly desirable.

In this context, the ternary intermetallic stannides such as $R_3T_4\text{Sn}_{13}$, where $R=$Sr, Ca and $T=$Ir, Rh [10,11], have attracted special attention due to the existence of a second-order structural phase transition below T^*, its putative coexistence with a SC state below T_C, and its suppression upon applying pressure or chemical substitution [12–21]. Conventional phonon-mediated BCS character of the superconductivity with s-wave symmetry has been established and confirmed in these systems by a range of experimental probes [12,16,22–25]. However, their resulting phase diagram is very suggestive of strong interplay between different order parameters and

remarkably resembles the phase diagrams of the heavily studied unconventional SC [3,5,26–28]. The role of these order parameters and whether they are coexisting, competing, or cooperating with each other are still a matter of debate.

$\text{Sr}_3\text{Ir}_4\text{Sn}_{13}$ and $\text{Ca}_3\text{Ir}_4\text{Sn}_{13}$ exhibit an anomaly in the temperature-dependent electrical resistivity and magnetic susceptibility measurements below $T^* \sim 147$ K and $T^* \sim 33$ K, followed by a SC transition at $T_C = 5$ K and $T_C = 7$ K, respectively [15]. Single-crystal x-ray diffraction and neutron-scattering measurements revealed that such anomaly is produced by a second-order structural phase transition from a simple cubic parent structure (space group $Pm\bar{3}n$ at 300 K), to a superlattice variant ($I\bar{4}3d$), where the lattice parameter is twice that of the room temperature phase [14,15]. The complete substitution of Sr by Ca, which corresponds to a positive pressure of ~ 5 GPa, reduces T^* and this behavior continues for the $(\text{Ca}_{1-x}\text{Sr}_x)_3\text{Ir}_4\text{Sn}_{13}$ series under external pressure. Full suppression of T^* is predicted at a structural quantum critical point ≈ 1.8 GPa for $\text{Ca}_3\text{Ir}_4\text{Sn}_{13}$ [15,16]. Several experimental probes suggest that such structural instability is associated with a charge density wave (CDW) transition involving the conduction electrons [15]. Such idea is supported by a decrease in the carrier density and the formation of a partial energy gap at the Fermi surface through the onset of the structural phase transition [29–33]. Moreover, muon spin relaxation measurements revealed a strong enhancement of the superfluid density and a dramatic increase of the pairing strength above ≈ 1.6 GPa, giving evidence of the

presence of a QCP [16]. Although several investigations have been realized on this system, in none of these experiments has the CDW been microscopically probed inside the SC phase and the question remains whether it survives in this low-temperature phase. Since the feature associated with the structural transition is weakened when approaching the QCP, a range of experimental probes has so far failed to identify it. In this sense, whether the CDW and SC states coexist and the exact pressure at which the CDW disappears are yet to be determined or confirmed.

With the improvement of x-ray diffraction (XRD) techniques to an extended pressure range it is now possible to explore the evolution of CDW modulation and its instabilities when approaching a pressure-driven QCP [34–36]. X-ray diffraction is a particularly valuable technique since it provides direct microscopic insight into the CDW modulation, allowing the determination of the CDW wave vector and the temperature and/or magnetic field dependencies of the order parameter and correlation lengths. Thus, its combination with high-pressure instrumentation provides a powerful tool for manipulating the nature of charge order in emergent materials.

Here, using high-energy x-ray diffraction measurements we have performed a detailed study of the evolution of the superlattice structure of $(Sr, Ca)_3Ir_4Sn_{13}$ against pressure and temperature. We find that the superlattice transition temperature T^* is rapidly suppressed with increasing pressure and extrapolates to zero at a critical pressure of $\approx 1.79(4)\,GPa$, in agreement with previous studies [15,16]. Our XRD measurements on $Ca_3Ir_4Sn_{13}$ revealed an anomaly related to a partial suppression of the superlattice peak intensity, which takes place at low temperatures ($T < 15$ K) and under pressures ($p > 0.09$ GPa). Such anomaly is also manifested by a large decrease of the static coherence length (ξ) when the temperature approaches zero. Since information about fluctuations can also be obtained from the Bragg diffraction peaks coming from a static order parameter, our results suggest that quantum fluctuation effects is likely the mechanism behind the destruction of the long-range CDW modulation in $Ca_3Ir_4Sn_{13}$. The presence of strong quantum fluctuations competing with CDW modulation and possibly with SC makes the phase diagram of $(Sr, Ca)_3Ir_4Sn_{13}$ reminiscent of unconventional SC.

II. SAMPLES AND METHODS

Single crystals of $(Sr, Ca)_3Ir_4Sn_{13}$ were grown by the flux method as described elsewhere [37]. The crystal structure and phase purity were determined by XRD on powdered crystals (not shown). Ambient pressure synchrotron XRD data ($E = 8.33$ keV) were collected on single crystals ($\approx 2 \times 1 \times 1$ mm^3) at beamline P09 at PETRA III, DESY [38]. The high quality of the crystal was verified by a mosaic spread of $0.01°$ determined at the $(0, 4, 1)$ Bragg reflection in the room temperature $Pm\bar{3}n$ phase.

A high-pressure single-crystal XRD experiment on $Ca_3Ir_4Sn_{13}$ was performed at the P07 beamline of PETRA III, DESY. A single crystal of $\sim 1 \times 1 \times 0.5$ mm^3 dimensions was cut and polished to achieve a flat and shiny surface perpendicular to the [001] direction. The measurements were performed using a clamp-type pressure cell [34] inserted in a 10 T cryomagnet installed on top of the triple-axis

diffractometer. Pressure calibration was determined by measuring the pressure dependence of the orthorhombic splitting of $(2, 0, 0)/(0, 2, 0)$ Bragg peaks on $La_{1.875}Ba_{0.125}CuO_4$ as described in Refs. [34,35]. Further details of the pressure calibration can be found in the Supplemental Material [39]. Daphne oil was used as a pressure-transmitting fluid. The bulk properties of the superlattice modulation as well as the crystal structure were studied by transmission geometry taking advantage of the large penetration depth and wide range of reciprocal space allowed by the high-energy photons ($E = 98.7$ keV). All crystal directions and scattering vectors, $\mathbf{Q} = (h, k, l)$, are specified in units of $(2\pi/a, 2\pi/b, 2\pi/c)$ of the room temperature cubic unit cell $Pm\bar{3}n$ ($a = b = c = 9.72$ Å). Access to the (h, k, l) Bragg and superlattice peaks was obtained by aligning either of the a-c axes horizontally, with the c axis approximately along the magnetic field and beam direction. The initial alignment of the single crystal was performed by collecting the diffraction patterns with a PerkinElmer detector; once the superlattice peaks were identified, a point detector was used (consisting of a broadband analyzer crystal and a scintillation counter).

A high-pressure single-crystal XRD experiment on $Sr_3Ir_4Sn_{13}$ was performed at the XDS beamline of the Brazilian Synchrotron Light Source (LNLS) [40]. The diamond anvil cell (DAC) was placed in the cold finger of a He closed-cycle cryostat and data were collected using a Pilatus 300 K detector. Due to the DAC limited angular scattering range ($25°$ of scattering angle 2θ), the beam was tuned to $E = 20$ keV in order to detect a significant number of Bragg peaks. The DAC was prepared with two full diamonds of $600\,\mu m$ culet size and a single crystal of $\sim 80 \times 80 \times 40\,\mu m^3$ was loaded together with ruby crystals for *in situ* pressure calibration and 4:1 methanol:ethanol as pressure media. The single-crystal XRD measurements were performed in transmission geometry, vertical scattering, with the c axis along the beam direction.

III. RESULTS

A. Ambient pressure XRD measurements

At ambient pressure, single-crystal XRD measurements on $Ca_3Ir_4Sn_{13}$ and $Sr_3Ir_4Sn_{13}$ reveal a series of satellite peaks below $T^* = 38.2(1)$ K and $T^* = 151.2(1)$ K, respectively, at $\mathbf{Q}_{SL} = \tau + \mathbf{q}_{SL}$, where τ is the wave vector of the room temperature phase and $\mathbf{q}_{SL} = (0.5, 0.5, 0)$ the propagation vector of the superlattice structure. No reflections associated with $\mathbf{q}_{SL} = (0.5, 0.5, 0.5)$ or $(0, 0, 0.5)$ modulations were found, in agreement with previous studies [14,41]. The propagation vector $\mathbf{q}_{SL} = (0.5, 0.5, 0)$ seems to be the benchmark in this 3-4-13 family of compounds, as it was also confirmed in $(Sr, Ca)_3Rh_4Sn_{13}$ [18], $La_3Co_4Sn_{13}$ [42], and even in $Eu_3Ir_4Sn_{13}$ [43], which also displays magnetic ordering at low temperatures. Figure 1 shows the temperature dependence of the integrated intensity for the superlattice reflections $(0, 4.5, 0.5)$ and $(3, 2.5, 0.5)$ for $Ca_3Ir_4Sn_{13}$ and $Sr_3Ir_4Sn_{13}$, respectively. A continuous decrease of the superlattice peak indicates a second-order phase transition at T^*. The temperature-dependent data were fitted by a power-law expression $\propto (1 - T/T^*)^{2\beta}$ yielding a critical exponent of $\beta = 0.30(1)$ for $Ca_3Ir_4Sn_{13}$ and $\beta = 0.29(1)$ for $Sr_3Ir_4Sn_{13}$, characteristics of a three-dimensional character transition.
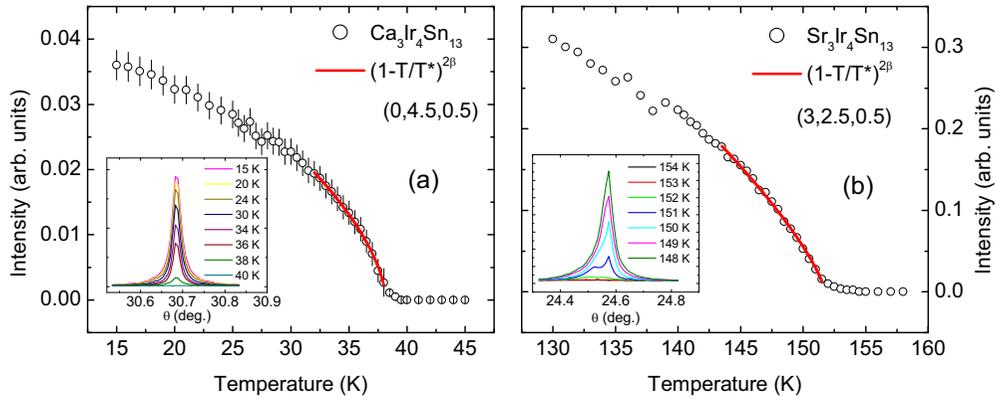
FIG. 1. Temperature dependence of the $(0, 4.5, 0.5)$ and $(3, 2.5, 0.5)$ superlattice reflections at ambient pressure for (a) $Ca_3Ir_4Sn_{13}$ and (b) $Sr_3Ir_4Sn_{13}$, respectively. The red solid line is a fitting using a power law to determine T^*. The insets show the rocking curves around the superlattice reflection measured for selected temperatures for each compound.

B. High-pressure XRD measurements on $Ca_3Ir_4Sn_{13}$

The temperature and pressure dependence of the superlattice peak $\mathbf{Q}_{SL} = (3, 1.5, 0.5)$ are summarized in Figs. 2(a)–2(f). The measurements consisted of rocking [Fig. 2(a)] and 2θ scans collected at several pressures and temperatures. At $p = 0.09$ GPa, the integrated intensity of the superlattice peak grows gradually on cooling below ∼32 K [see Fig. 2(b)]. A saturation of the peak intensity seems to take place below the superconducting temperature $T_C \sim 7$ K, as also observed at ambient pressure. Interestingly, for pressures higher than
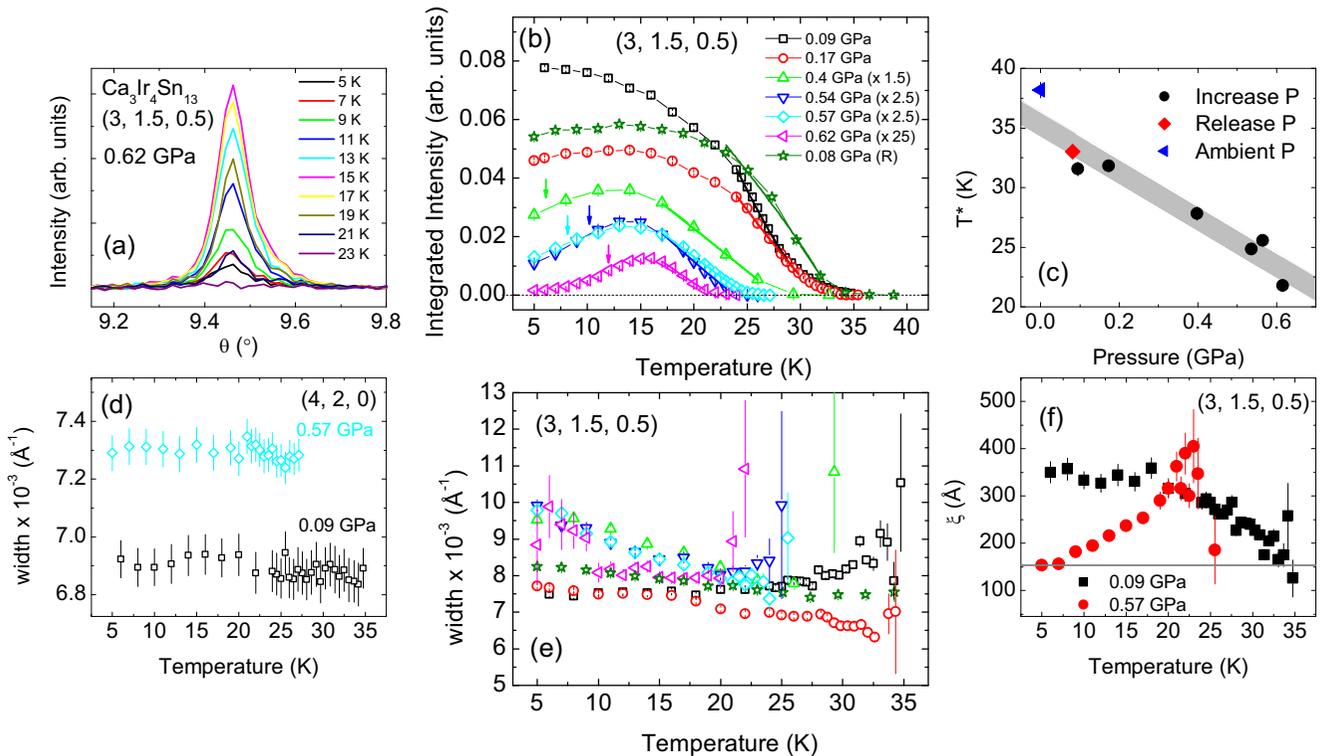
FIG. 2. (a) Evolution of the $(3, 1.5, 0.5)$ superlattice peak intensity at $p = 0.62$ GPa. (b) Temperature dependence of the $(3, 1.5, 0.5)$ superlattice peak intensity at several pressures. Thin solid lines are guides to the eye. Thick solid lines are the fittings to the power law $\propto (1 - T/T^*)^{2\beta}$. The arrows indicate the value of T', extracted from the maximum of the first derivative of the superlattice peak intensity with respect to temperature (see Ref. [39] for further details). The pressure dependence of T^* for $Ca_3Ir_4Sn_{13}$ is shown in (c). (d), (e) Evolution of the pseudo-Voigt linewidth against temperature at selected pressures for $(4, 2, 0)$ Bragg and $(3, 1.5, 0.5)$ superlattice peaks, respectively, extracted from 2θ scans. (f) Temperature dependence of the static correlation length, ξ, of the $(3, 1.5, 0.5)$ superlattice reflection at $p = 0.09$ GPa and $p = 0.57$ GPa. The gray line indicates the similar correlation lengths observed at $T = 5$ K and $p = 0.57$ GPa and at $T \sim 32$ K and $p = 0.09$ GPa. Details of the calculation of the correlation length can be found in Ref. [39]. The estimated pressure error bar is ± 0.1 GPa.

$p \sim 0.17$ GPa, the superlattice peak intensity is partially suppressed below $T \sim 15$ K. This suppression is enhanced upon pressure increase up to $p = 0.62$ GPa, above which total suppression of the superlattice peak intensity is observed (see Fig. S1 in the Supplemental Material [39] for the $p = 0.7$ GPa data set). The temperature dependence of the superlattice peak intensity for different pressures [Fig. 2(b)] was fitted by a power law $\propto (1 - T/T^*)^{2\beta}$ and the best fit to the data near T^* corresponds to the critical temperatures displayed in Fig. 2(c).

Further insight into the partial suppression of the superlattice peak intensity is given by the temperature dependence of the pseudo-Voigt linewidths. The linewidths were extracted from the 2θ scans at the lattice and superlattice Bragg peaks $(4, 2, 0)$ and $(3, 1.5, 0.5)$, respectively [Figs. 2(d) and 2(e), respectively]. At ambient pressure, the superlattice peak is resolution limited, while it develops a small but finite width at 0.09 GPa (correlation length of $\xi \sim 340$ Å) indicating the CDW is long-range ordered (see Supplemental Material [39]). At low pressures ($p \lesssim 0.17$ GPa), the linewidth of the superlattice modulation [Fig. 2(e)] is comparable to that of the Bragg reflection [Fig. 2(d)] and is mostly temperature-independent at low temperatures. Upon further pressure increase, the linewidth increases 30% from $p = 0.09$ GPa to $p = 0.57$ GPa at $T = 5$ K. Surprisingly, the widths at low temperatures ($T \sim 5$ K, $p = 0.54$–0.62 GPa) are comparable to the values observed in proximity to the structural phase transition ($T^* \sim 20$–32 K, $p = 0.09$–0.62 GPa), indicating that a competing order of similar energy scales is likely to be developing at low temperatures and high pressures. This same feature is highlighted in Fig. 2(f), where the temperature dependence of the correlation length of the superlattice peak $(3, 1.5, 0.5)$ for two different pressures is plotted: a correlation length of $\xi \sim 153$ Å can be observed in either $T = 5$ K and $p = 0.57$ GPa or $p = 0.09$ GPa and $T \sim 32$ K curves.

We have also explored the crystal structure of $Ca_3Ir_4Sn_{13}$ under pressure. The evolution of the cubic lattice parameter a at $T = 5$ K was obtained through the analysis of selected structural Bragg peaks [$(0, 0, 4)$ and $(4, 2, 0)$]. Within our experimental accuracy, no discontinuities in lattice parameters or signatures of a structural phase transition were found in the entire pressure range measured [Fig. 3(a)]. Such lattice constant is well characterized by a single-parameter Birch equation of state (EoS) with bulk modulus of $B = 72(13)$ GPa and a-axis compression rate of $\frac{\Delta a/a_0}{\Delta P} = -0.4(1)$ %/GPa, where a_0 is the lattice parameter at $p = 0.09$ GPa.

In order to verify whether the partial suppression of the superlattice intensity is due to a competition between CDW and superconductivity, we have probed the effect of application of magnetic field on the superlattice modulation. A maximum field of 9 T was applied along the $\mathbf{Q}_{SL} = (3, 1.5, 0.5)$ direction. The field dependence of the intensity of the superlattice reflection $(3, 1.5, 0.5)$ at $T = 5$ K is shown in Fig. 3(b). Application of a magnetic field has no significant effect, considering the experimental errors, on the superlattice peak intensity. We note that previous studies [13,44] report that the upper critical field is $H_c \approx 7$ T and does not vary significantly under pressure, so a magnetic field of $\mu_0 H = 9$ T is enough to suppress the superconductivity in this material
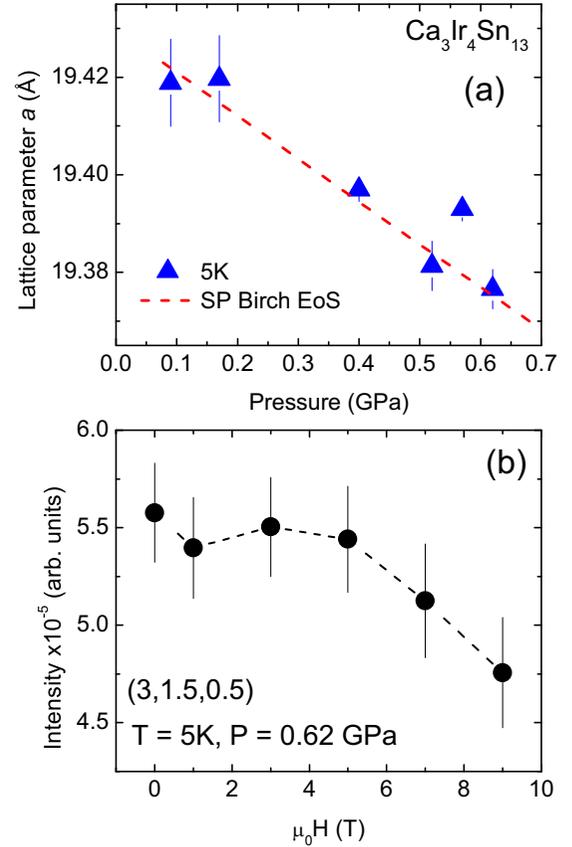
FIG. 3. (a) Pressure dependence of the lattice parameter a extracted from lattice Bragg reflections in the low-temperature $I\bar{4}3d$ space group and its fit to a single parameter Birch equation of state (EoS). (b) Magnetic field dependence of the superlattice modulation peak intensity at $(3, 1.5, 0, 5)$ for $T = 5$ K and $p = 0.62$ GPa. The data set was collected with a magnetic field applied along $\mathbf{Q}_{SL} = (3, 1.5, 0.5)$ direction.

at $p = 0.66$ GPa, where the normal state is disclosed down to 2 K.

C. High-pressure XRD measurements on $Sr_3Ir_4Sn_{13}$

A detailed single-crystal XRD study under pressure was conducted on the $Sr_3Ir_4Sn_{13}$ compound. Figure 4(a) displays the temperature dependence of the intensity at several superlattice peaks under pressure. As expected from the high-pressure electrical resistivity measurements [15], a drastic suppression of the superlattice transition temperature is observed. The temperature dependence of the superlattice peak intensity was also fitted by the power law $\propto (1 - T/T^*)^{2\beta}$ and the best fit to the data near T^* corresponds to the critical temperatures displayed in the phase diagram of Fig. 5. Figure 4(b) shows the evolution of the intensity of the superlattice peak $(3, 2.5, 0.5)$ normalized by the Bragg reflection $(3, 2, 0)$ against pressure. Due to temperature constraints ($T_{min} \sim 40$ K), the superlattice peak intensity was probed up to the highest pressure of ~ 4.6 GPa. The total superlattice peak suppression is expected to take place at ≈ 7.7 GPa based on the linear extrapolation of the pressure evolution of T^*, as will be discussed below.
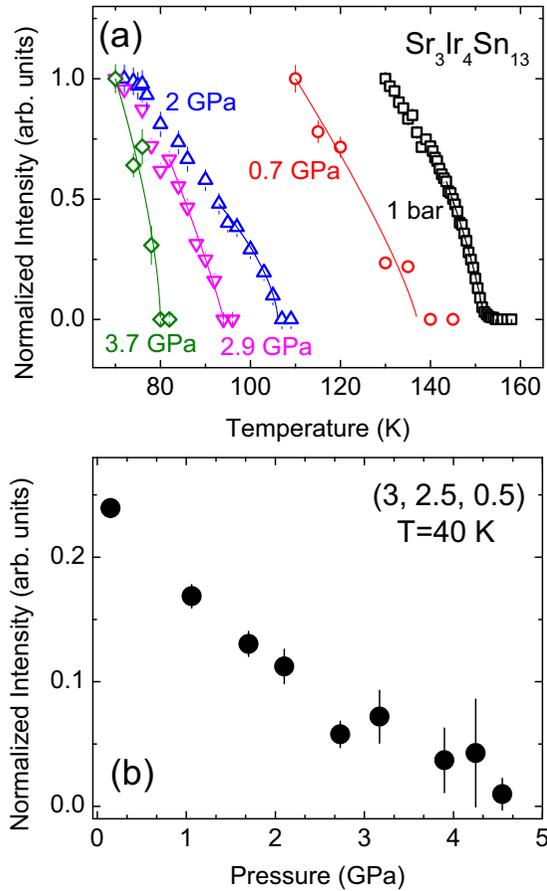
FIG. 4. (a) Temperature dependence of several superlattice peaks [(3, 1.5, −0.5), (3, 2.5, 0.5), and (2.5, 1, −0.5)] of $Sr_3Ir_4Sn_{13}$ at selected pressures. The data set was normalized to one due to intensity differences among the reflections probed. Solid lines are the fittings to the power law $\propto (1 - T/T^*)^{2\beta}$. (b) Pressure dependence of the (3, 2.5, 0.5) superlattice peak integrated intensity at 40 K, which was normalized by the (3, 2, 0) Bragg reflection.

FIG. 5. Phase diagram of the $(Ca_xSr_{1-x})_3Ir_4Sn_{13}$ system proposed by the present high-energy and high-pressure XRD measurements. Based on our data (open diamonds and circles for the XRD data and open circles with dot for the electrical resistivity), the superlattice transition temperature, T^*, extrapolates to zero at ∼1.79(4) GPa. Closed green circles are T_C values determined from resistivity measurements [39]. Star symbols (T') are the temperatures where the quantum fluctuations emerge. The open and closed left black triangles are the T^* and T_C values, respectively, from resistivity measurements of Refs. [15]. Blue triangles are T_C values obtained from μSR measurements from Ref. [16].

IV. DISCUSSION

It has been shown that the combination of physical and chemical pressure has strong influence on the superlattice phase of the 3-4-13 series of compounds, such as the $(Ca_xSr_{1-x})_3Ir_4Sn_{13}$, where bulk measurements reveal a suppression of the second-order structural phase transition at T^* [14–16]. Our XRD measurements on $(Sr, Ca)_3Ir_4Sn_{13}$ constitute a detailed structural study of this class of material under pressure, contributing to the advancement of the temperature-pressure phase diagram, which up to now has been based solely on electrical resistivity, magnetic susceptibility, muon spin relaxation, and nuclear magnetic resonance measurements [15,16,28].

Among the $(Ca_xSr_{1-x})_3Ir_4Sn_{13}$ series at ambient pressure, $Ca_3Ir_4Sn_{13}$ displays the smallest difference between its order parameters ($T^* \sim 38$ K and $T_C \sim 7$ K at ambient pressure) and is thus more prone to external stimuli, such as applied physical pressure. Indeed, our high-energy, high-pressure XRD measurements on $Ca_3Ir_4Sn_{13}$ reveal that T^* is rapidly suppressed by pressure at a rate of $dT^*/dP \approx -19.3 \pm 0.3$ K/GPa, with the superlattice modulation intensity van-

ishing completely above ∼0.62 GPa. Such result corroborates with our resistivity measurements, where the resistivity anomaly associated with T^* was last seen at $T^* \sim 21(1)$ K and $p = 0.55(5)$ GPa. Combined with the high-pressure XRD data on $Sr_3Ir_4Sn_{13}$, T^* extrapolates to zero at a critical pressure of $p_c \sim 1.79(4)$ GPa (black filled half circle in Fig. 5), in striking agreement with values found in the literature [15,16].

Interesting to note is the pressure-induced partial suppression of the superlattice peak intensity for temperatures below 15 K [Fig. 2(b)]. Such anomaly is also manifested in the pseudo-Voigt linewidth as a function of temperature for selected pressures [Fig. 2(e)]. Closer to ambient pressure, the linewidth has little to no dependence on temperature. For $p > 0.09$ GPa and $T < 15$ K, the CDW modulation becomes less long-range ordered, with Q_{SL} width increasing when temperature is lowered to $T \sim 5$ K. Figure 2(f) shows the correlation length of the CDW modulation, which decreases from $\xi \sim 341$ Å at $p = 0.09$ GPa to 153 Å at $p = 0.62$ GPa at $T \sim 5$ K, a reduction of 55% (going from ∼17.6 to ∼8 CDW wavelengths [45]). Our results strongly suggest that a competing order of similar energy scales is developing at low temperatures and high pressures. The possible nature of such order parameter and its implications will be discussed below.

Our XRD investigation on the evolution of the lattice parameter against pressure reveals no sign of a structural phase transition within our experimental accuracy, suggesting that the crystal structure remains within the superlattice variant unit cell $I\bar{4}3d$. This was further supported by the pseudo-Voigt linewidths extracted from the lattice Bragg

peaks: a 5% peak broadening was found from $p = 0.09$ to 0.57 GPa, but such value is likely attributed to the natural peak broadening related to application of pressure rather than to the onset of a structural phase transition. From the field-dependent data shown in Fig. 3(b), we found that an applied magnetic field of 9 T, at $T = 5$ K, along $Q_{SL} = (3, 1.5, 0.5)$, which should be enough to suppress the superconducting phase in $Ca_3Ir_4Sn_{13}$ [44], has no significant effect on the superlattice modulation intensity. This is in contrast with observations in cuprate materials, such as $YBa_2Cu_3O_{6.67}$ [36], where application of magnetic field suppresses superconductivity and enhances the spontaneous CDW ordering with wave vector $q_{CDW} = q_1 = (\delta_1, 0, 0.5)$ and $q_2 = (0, \delta_2, 0.5)$, with $\delta_1 = 0.3045(2)$ and $\delta_2 = 0.3146(7)$.

It should be noted that fluctuation effects [6,46,47] might be playing a crucial role in the decrease in coherence length of the CDW modulation at $T < 15$ K and $p > 0.09$ GPa. Analysis of the linewidth of the 2θ scans indicates that at $p = 0.09$ GPa the profile shape is mostly Gaussian and evolves toward Lorentzian when approaching the superlattice phase transition at T^* (see Figs. S4 and S5 in the Supplemental Material [39]). For higher pressures, on the other hand, the profile shape has a significant contribution from the Lorentzian line shape, indicating that the superlattice phase correlation is exponentially decaying in real space already at low temperatures [46,47]. This result could be consistent with a disorder pinning scenario [48–50], where the CDW phase distortion is distributed over a spatial range across the pinning site [49]. However the short correlation length (~ 8 unit cells) observed at $p = 0.62$ GPa is unlikely to accommodate several disorder sites within a coherent volume to pin the CDW domain [47]. Thus, we believe that the mechanism for destroying the long-range CDW modulation in $Ca_3Ir_4Sn_{13}$ is probably the increasing quantum fluctuations when $T \to 0$ K and $p \to p_c$. Indeed, muon spin relaxation measurements [16] have pointed out the importance of fluctuations when approaching the quantum critical point, which might be the origin of the enhancement of the superconducting phase above p_c. Quantum fluctuations have also been highlighted in the $LuPt_{2-x}Pd_xIn$ system, where T_C presents a dome-shaped doping dependence with the highest value exactly where the CDW transition disappears [6]. Moreover, a recent study of the CDW order parameter critical exponent in cubic intermetallics, including the $(Ca_{1-x}Sr_x)_3Ir_4Sn_{13}$ family of compounds, reveals a crossover of the classical thermal-driven CDW order parameter critical exponent expected for a three-dimensional universality class ($\beta \approx 0.3$) to a mean-field tendency ($\beta \approx 0.5$) as $T^* \to 0$ [51]. This mean-field-like phenomenology supports the increase of dimensionality due to quantum fluctuations and provides evidence for the existence of a QCP in these compounds.

Finally, we have constructed the temperature-pressure phase diagram of Fig. 5. Results from XRD measurements on $(Sr, Ca)_3Ir_4Sn_{13}$, electrical resistivity experiments on $Ca_3Ir_4Sn_{13}$, as well as other studies found in the literature are reported. The phase diagram also depicts the apparent short-range order phase related to the partial suppression of the superlattice peak intensity in $Ca_3Ir_4Sn_{13}$ and possibly to the quantum fluctuations in this material. To better follow the evolution of such phase, we have extracted

the temperature T' from the maximum of the first derivative of the temperature dependence of the superlattice peak intensity for $T < 15$ K (see Fig. S6 of the Supplemental Material [39] for more details). As mentioned before, our results suggests an enhancement of the quantum fluctuations when $T \to 0$ K and $p \to p_c$, which is likely the mechanism behind the partial/total suppression of the superlattice modulation at low temperatures. Although not probed in our experiment, we believe that a reentrant CDW modulation at higher pressures is unlikely to happen due to the lack of observation of such feature in bulk measurements. The presence of quantum fluctuations competing with CDW modulation and possibly with superconductivity makes the phase diagram of $(Sr, Ca)_3Ir_4Sn_{13}$ reminiscent of unconventional superconductors. Indeed, it has been reported that these systems also show some unusual properties similar to the Fe-pnictide high-temperature superconductors [28], providing further evidence of the rich phase diagrams displayed by these materials. Particularly for $Ca_3Ir_4Sn_{13}$, the different types of orders occur on comparable temperature scales and can compete/cooperate on an almost equal footing revealing their intertwined nature. Further experimental efforts will help to determine more accurately the *P-T* phase diagram as well as the nature of the quantum fluctuations in the low-temperature, high-pressure phase. For instance, measurements of the diffuse elastic linewidth in the anomalous phase could determine the critical exponent that controls the correlation length of the fluctuations.

V. CONCLUSION

Here we have performed a detailed study of the evolution of the superlattice structure of $(Sr, Ca)_3Ir_4Sn_{13}$ against pressure by means of high-energy XRD measurements. We found that the superlattice transition temperature T^* is rapidly suppressed with increasing pressure and extrapolates to zero at a critical pressure of $p_c \sim 1.79(4)$ GPa. Our XRD measurements on $Ca_3Ir_4Sn_{13}$ revealed an anomaly related to a partial suppression of the superlattice peak intensity, which takes place at low temperatures ($T < 15$ K) and high pressures ($p > 0.09$ GPa). Such anomaly is also manifested by an increase of the pseudo-Voigt linewidth of the 2θ scans when the temperature approaches zero. With no apparent origin on a structural phase transition or a competition with the superconducting phase that emerges at $T_C \sim 7$ K and reaches its maximum at $p \sim 4$ GPa, our results suggest that quantum fluctuation effects are possibly the mechanism behind the destruction of the long-range CDW modulation. The revisited temperature-pressure phase diagram of $(Sr, Ca)_3Ir_4Sn_{13}$ highlights the intertwined nature of the distinct order parameters and demonstrates some similarities of this family of supposedly conventional BCS superconductors [12,16,22–24] and the unconventional superconductors.

[1] E. Fradkin, S. A. Kivelson, and J. M. Tranquada, Rev. Mod. Phys. **87**, 457 (2015).

[2] D. J. Scalapino, Rev. Mod. Phys. **84**, 1383 (2012).

[3] J. Paglione and R. L. Greene, Nat. Phys. **6**, 645 (2010).

[4] B. Keimer, S. A. Kivelson, M. R. Norman, S. Uchida, and J. Zaanen, Nature (London) **518**, 179 (2015).

[5] P. Gegenwart, Q. Si, and F. Steglich, Nat. Phys. **4**, 186 (2008).

[6] T. Gruner, D. Jang, Z. Huesges, R. Cardoso-Gil, G. H. Fecher, M. M. Koza, O. Stockert, A. P. Mackenzie, M. Brando, and C. Geibel, Nat. Phys. **13**, 967 (2017).

[7] P. Monthoux, D. Pines, and G. G. Lonzarich, Nature (London) **450**, 1177 (2007).

[8] N. D. Mathur, F. M. Grosche, S. R. Julian, I. R. Walker, D. M. Freye, R. K. W. Haselwimmer, and G. G. Lonzarich, Nature (London) **394**, 39 (1998).

[9] E. Slooten, T. Naka, A. Gasparini, Y. K. Huang, and A. de Visser, Phys. Rev. Lett. **103**, 097003 (2009).

[10] J. P. Remeika, G. P. Espinosa, A. S. Cooper, H. Barz, J. M. Rowell, D. B. McWhan, J. M. Vandenberg, D. E. Moncton, Z. Fisk, L. D. Woolf, H. C. Hamaker, M. B. Maple, G. Shirane, and W. Thomlinson, Solid State Commun. **34**, 923 (1980).

[11] G. P. Espinosa, Mater. Res. Bull. **15**, 791 (1980).

[12] N. Kase, H. Hayamizu, and J. Akimitsu, Phys. Rev. B **83**, 184509 (2011).

[13] S. Y. Zhou, H. Zhang, X. C. Hong, B. Y. Pan, X. Qiu, W. N. Dong, X. L. Li, and S. Y. Li, Phys. Rev. B **86**, 064504 (2012).

[14] D. G. Mazzone, S. Gerber, J. L. Gavilano, R. Sibille, M. Medarde, B. Delley, M. Ramakrishnan, M. Neugebauer, L. P. Regnault, D. Chernyshov, A. Piovano, T. M. Fernández-Díaz, L. Keller, A. Cervellino, E. Pomjakushina, K. Conder, and M. Kenzelmann, Phys. Rev. B **92**, 024101 (2015).

[15] L. E. Klintberg, S. K. Goh, P. L. Alireza, P. J. Saines, D. A. Tompsett, P. W. Logg, J. Yang, B. Chen, K. Yoshimura, and F. M. Grosche, Phys. Rev. Lett. **109**, 237008 (2012).

[16] P. K. Biswas, Z. Guguchia, R. Khasanov, M. Chinotti, L. Li, K. Wang, C. Petrovic, and E. Morenzoni, Phys. Rev. B **92**, 195122 (2015).

[17] W. C. Yu, Y. W. Cheung, P. J. Saines, M. Imai, T. Matsumoto, C. Michioka, K. Yoshimura, and S. K. Goh, Phys. Rev. Lett. **115**, 207003 (2015).

[18] Y. W. Cheung, Y. J. Hu, M. Imai, Y. Tanioku, H. Kanagawa, J. Murakawa, K. Moriyama, W. Zhang, K. T. Lai, K. Yoshimura, F. M. Grosche, K. Kaneko, S. Tsutsui, and S. K. Goh, Phys. Rev. B **98**, 161103(R) (2018).

[19] S. K. Goh, D. A. Tompsett, P. J. Saines, H. C. Chang, T. Matsumoto, M. Imai, K. Yoshimura, and F. M. Grosche, Phys. Rev. Lett. **114**, 097002 (2015).

[20] C. S. Lue, C. N. Kuo, C. W. Tseng, K. K. Wu, Y.-H. Liang, C.-H. Du, and Y. K. Kuo, Phys. Rev. B **93**, 245119 (2016).

[21] Y. W. Cheung, Y. J. Hu, S. K. Goh, K. Kaneko, S. Tsutsui, P. W. Logg, F. M. Grosche, H. Kanagawa, Y. Tanioku, M. Imai, T. Matsumoto, and K. Yoshimura, J. Phys.: Conf. Ser. **807**, 032002 (2017).

[22] S. Gerber, J. L. Gavilano, M. Medarde, V. Pomjakushin, C. Baines, E. Pomjakushina, K. Conder, and M. Kenzelmann, Phys. Rev. B **88**, 104505 (2013).

[23] P. K. Biswas, A. Amato, R. Khasanov, H. Luetkens, K. Wang, C. Petrovic, R. M. Cook, M. R. Lees, and E. Morenzoni, Phys. Rev. B **90**, 144505 (2014).

[24] P. K. Biswas, A. Amato, K. Wang, C. Petrovic, R. Khasanov, H. Luetkens, and E. Morenzoni, J. Phys.: Conf. Ser. **551**, 012029 (2014).

[25] H. Hayamizu, N. Kase, and J. Akimitsu, Phys. C (Amsterdam) **470**, S541 (2010).

[26] K. Hashimoto, K. Cho, T. Shibauchi, S. Kasahara, Y. Mizukami, R. Katsumata, Y. Tsuruhara, T. Terashima, H. Ikeda, M. A. Tanatar, H. Kitano, N. Salovich, R. W. Giannetta, P. Walmsley, A. Carrington, R. Prozorov, and Y. Matsuda, Science **336**, 1554 (2012).

[27] T. Shibauchi, A. Carrington, and Y. Matsuda, Annu. Rev. Condens. Matter Phys. **5**, 113 (2014).

[28] J. Luo, J. Yang, S. Maeda, Z. Li, and G.-Q. Zheng, Chin. Phys. B **27**, 077401 (2018).

[29] C. N. Kuo, H. F. Liu, C. S. Lue, L. M. Wang, C. C. Chen, and Y. K. Kuo, Phys. Rev. B **89**, 094520 (2014).

[30] L. M. Wang, C.-Y. Wang, G.-M. Chen, C. N. Kuo, and C. S. Lue, New J. Phys. **17**, 033005 (2015).

[31] K. Wang and C. Petrovic, Phys. Rev. B **86**, 024522 (2012).

[32] A. F. Fang, X. B. Wang, P. Zheng, and N. L. Wang, Phys. Rev. B **90**, 035115 (2014).

[33] B. Chen, J. Yang, Y. Guo, and K. Yoshimura, Europhys. Lett. **111**, 17005 (2015).

[34] M. v. Zimmermann, R. Nowak, G. D. Gu, C. Mennerich, H.-H. Klauss, and M. Hücker, Rev. Sci. Instrum. **79**, 033906 (2008).

[35] M. Hücker, M. v. Zimmermann, M. Debessai, J. S. Schilling, J. M. Tranquada, and G. D. Gu, Phys. Rev. Lett. **104**, 057004 (2010).

[36] J. Chang, E. Blackburn, A. T. Holmes, N. B. Christensen, J. Larsen, J. Mesot, R. Liang, D. A. Bonn, W. N. Hardy, A. Watenphul, M. v. Zimmermann, E. M. Forgan, and S. M. Hayden, Nat. Phys. **8**, 871 (2012).

[37] C. Israel, E. M. Bittar, O. E. Agüero, R. R. Urbano, C. Rettori, I. Torriani, P. G. Pagliuso, N. O. Moreno, J. D. Thompson, M. F. Hundley, J. L. Sarrao, and H. A. Borges, Phys. B Condensed Matter **359-361**, 251 (2005).

[38] J. Strempfer, S. Francoual, D. Reuther, D. K. Shukla, A. Skaugen, H. Schulte-Schrepping, T. Kracht, and H. Franz, J. Synchrotron Radiat. **20**, 541 (2013).

[39] See Supplemental Material at http://link.aps.org/supplemental/10.1103/PhysRevB.101.104511 for further information on the raw XRD data at $p = 0.7$ GPa, the pressure calibration using $La_{1.875}Ba_{0.125}CuO_4$, the analysis of the line shape of the 2θ scans and resistivity measurements. The Supplemental Material includes Ref. [52].

[40] F. A. Lima, M. E. Saleta, R. J. S. Pagliuca, M. A. Eleotério, R. D. Reis, J. Fonseca Júnior, B. Meyer, E. M. Bittar, N. M. Souza-Neto, and E. Granado, J. Synchrotron Radiat. **23**, 1538 (2016).

[41] D. A. Tompsett, Phys. Rev. B **89**, 075117 (2014).

[42] L. Mendonça-Ferreira, F. B. Carneiro, M. B. Fontes, E. Baggio-Saitovitch, L. S. I. Veiga, J. R. L. Mardegan, J. Strempfer, M. M. Piva, P. G. Pagliuso, R. D. dos Reis, and E. M. Bittar, J. Alloys Compd. **773**, 34 (2019).

[43] J. R. L. Mardegan, N. Aliouane, L. N. Coelho, O. Agüero, E. M. Bittar, J. C. Lang, P. G. Pagliuso, I. L. Torriani, and C. Giles, IEEE Trans. Magn. **49**, 4652 (2013).

[44] S. K. Goh, L. E. Klintberg, P. L. Alireza, D. A. Tompsett, J. Yang, B. Chen, K. Yoshimura, and F. M. Grosche, arXiv:1105.3941.

[45] The lattice parameter used here corresponds to the body-centered space group, where lattice constants are double of the room temperature cubic unit cell $Pm\bar{3}n$. Value extracted from evolution of the lattice parameters against pressure at $T = 5$ K.

[46] Y. Feng, J. Wang, R. Jaramillo, J. van Wezel, S. Haravifard, G. Srajer, Y. Liu, Z.-A. Xu, P. B. Littlewood, and T. F. Rosenbaum, Proc. Natl. Acad. Sci. USA **109**, 7224 (2012).

[47] Y. Feng, J. van Wezel, J. Wang, F. Flicker, D. M. Silevitch, P. B. Littlewood, and T. F. Rosenbaum, Nat. Phys. **11**, 865 (2015).

[48] J. P. Hill, G. Helgesen, and D. Gibbs, Phys. Rev. B **51**, 10336 (1995).

[49] H. Fukuyama and P. A. Lee, Phys. Rev. B **17**, 535 (1978).

[50] D. DiCarlo, R. E. Thorne, E. Sweetland, M. Sutton, and J. D. Brock, Phys. Rev. B **50**, 8288 (1994).

[51] F. B. Carneiro, L. S. I. Veiga, J. R. L. Mardegan, R. Khan, C. Macchiutti, A. Lopez, and E. M. Bittar, arXiv:1912.05669.

[52] H. Takahashi, H. Shaked, B. A. Hunter, P. G. Radaelli, R. L. Hitterman, D. G. Hinks, and J. D. Jorgensen, Phys. Rev. B **50**, 3221 (1994).